J. Appl. Cryst. (1997). **30**, 16–20

A High-Energy Monochromatic Laue (MonoLaue) X-ray Diffuse Scattering Study of $KMnF_3$ using an Image Plate

A. GIBAUD,[a]* D. HARLOW,[b] J. B. HASTINGS,[c] J. P. HILL[c] AND D. CHAPMAN[c]

[a]*Argonne National Laboratory, 9700 South Cass Avenue, Argonne, Illinois 60439, USA,* [b]*E. I. Dupont De Nemours and Company, Wilmington, DE 19880-0228, USA, and* [c]*Brookhaven National Laboratory, Upton, Long Island, NY 11973, USA*

(*Received 13 September 1995; accepted 15 January 1996*)

Abstract

The technique of high-energy monochromatic Laue X-ray scattering using image plates to record the diffraction patterns is presented. A tunable wiggler beamline is used as an X-ray source. It is shown that such experimental conditions present many advantages over conventional tube sources and photographic films. A study of diffuse scattering in the perovskite compound $KMnF_3$ is presented to illustrate this in a qualitative way.

1. Introduction

In the past, the X-ray monochromatic laue (monoLaue) technique using conventional tube sources has been shown to be a very powerful tool for mapping out large regions of reciprocal space (Comes, Lambert & Guinier, 1970; Dénoyer, Comès & Lambert, 1970; Dénoyer, Comès, Lambert & Guinier, 1974; Gibaud, Bulou, Launay & Nouet, 1987). In this method, the incident beam is monochromatic, the crystal is kept in a fixed position (or is slightly oscillated) and the diffraction pattern is recorded on a film located a few centimetres away from the crystal, as shown in Fig. 1. In particular, the technique has proven to be invaluable in investigations of the anisotropy of diffuse scattering, whether of static or dynamic origin, in various materials such as metallic alloys and ionic crystals. However, with the development of counters, the use of film has rapidly decreased and the technique has only been used in a limited number of cases, despite its utility. Moreover, in its conventional form, the technique has a number of limitations. In order to get quantitative information from photographic films, it is necessary to use microdensitometers and to rely upon uniform film processing, which is usually fairly difficult and inconvenient. In addition, conventional tube sources have the drawback that they give strong lines at only a limited number of wavelengths. The most widely used sources are copper and molybdenum tubes, which produce radiation at their $K\alpha$ emission lines of 1.54 and 0.709 Å, respectively. These wavelengths are quite large, so that the radius of the Ewald sphere is correspondingly small. As a result, the interpretation of the monoLaue patterns is not trivial, as several Bragg sheets intercept the Ewald sphere simultaneously. Furthermore, the fact that many elements strongly absorb the incident beam and can present high fluorescence at these energies provides additional restrictions on the applicability of the technique. For instance, it is impossible to record the diffraction pattern of samples like $KMnF_3$ using Cu $K\alpha$ radiation, owing to the fluorescence of the manganese and because thin samples (about a hundred micrometres) are required even if one is working with Mo $K\alpha$ radiation. Another limitation comes from the limited space available between the sample and the film, which can be as small as a few centimetres in the case of the Cu $K\alpha$ radiation. Finally, even in cases for which these limitations are not restrictive, the low brightness of conventional sources leads to typical exposures of the order of 10 h.

The purpose of this work is to demonstrate that the limitations of the conventional monoLaue technique may now be circumvented. This is made possible by two recent technological advances. The first is the availability of high-brightness tunable high-energy wiggler sources at current-generation synchrotrons. The second is the

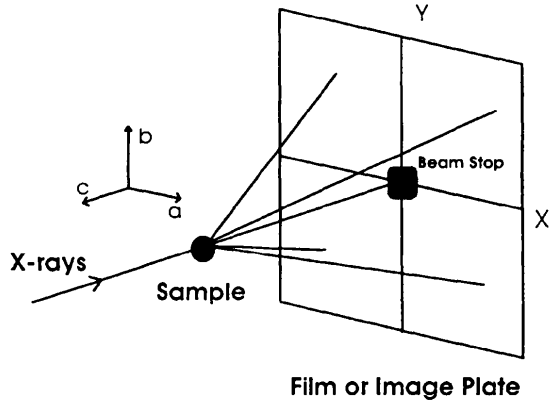

Fig. 1. Schematic representation of the monoLaue experimental set-up.

* Permanent and correspondence address: Université du Maine, Faculté des Sciences, URA 807 CNRS, 72017 Le Mans CEDEX, France.

© 1997 International Union of Crystallography
Printed in Great Britain – all rights reserved

development of image plates to record the diffraction patterns. As we shall see, the combination of these two advances dramatically improves the applicability of the monoLaue technique and makes it one of great power for the study of diffuse scattering. In this paper, we present the first X-ray scattering study of diffuse scattering along the RM line in $KMnF_3$ as a function of temperature, as an example of what can be achieved under such experimental conditions.

2. Experimental details

The experiments were performed at the National Synchrotron Light Source (NSLS, Brookhaven National Laboratory) at the X17B1 Wiggler Beam Line. The energy was tuned to 60 keV using an Si (220) Laue–Bragg two-crystal monochromator. The wavelength was determined using the location of the powdered-silicon diffraction lines. The incoming beam was collimated to a 1 mm^2 spot and a beam stop was placed between the sample and the image plate. The incident intensity was 1×10^9 photons s^{-1} at 200 mA of stored electron current. The sample was mounted in a cryogenerator and the image plate located 60 cm away from the sample, demonstrating the fact that the space limitation is no longer a problem at this energy. The beam-stop location was found to be critical in reducing the background. In order to get reliable intensities on the image plate, it was necessary to make $\pm 4°$ oscillations of the sample. Exposure times as short as 150 s saturated the image plate at the Bragg peak locations and produced clearly visible diffuse patterns.

The great advantage of working at such energies is that the Ewald sphere is essentially flat over the plane of recording media, as is the case, for instance, in electron diffraction. One can thus record similar patterns to those recorded with this latter technique, but X-ray diffraction offers two significant advantages. First, it is not surface sensitive (at 60 keV) and sample preparation is no longer of such concern. Second, there is no deleterious effect due to the incident-beam intensity at the surface. The sample thickness can be extremely large: in our case it was 3 mm. Since the Ewald sphere is nearly flat, there is only one scattering plane recorded at a time on the image plate, provided that the distance between the image plate and the sample is large enough. As we shall see below, lines of constant indices are nearly straight, which makes the interpretation of the pattern quite straightforward.

3. Discussion and results

The general aspect of a recorded pattern on a flat film can be understood in terms of the lines of constant indices. As previously reported (Gibaud, Bulou, Launay & Nouet, 1987; Gibaud, 1987), these lines represent the projection, on the flat surface of the film, of the intersection of reciprocal planes with the Ewald sphere, and lead to the so-called indexation diagrams. If we restrict ourselves to the simple case of a sample of orthorhombic symmetry lying with its c axis parallel to the direct beam and with the a axis in the horizontal plane, then the lines of constant h and k indices have x and y coordinates on the film given by:

$$x(h,k) = Dh \Big/ a\left(\frac{h^2}{a^2}+\frac{k^2}{b^2}\right)^{1/2} \times \tan\left\{\arcsin\left[\lambda\left(\frac{h^2}{a^2}+\frac{k^2}{b^2}\right)^{1/2}\right]\right\},$$

$$y(h,k) = Dk \Big/ b\left(\frac{h^2}{a^2}+\frac{k^2}{b^2}\right)^{1/2} \tan\left\{\arcsin\left[\lambda\left(\frac{h^2}{a^2}+\frac{k^2}{b^2}\right)\right]\right\}, \quad (1)$$

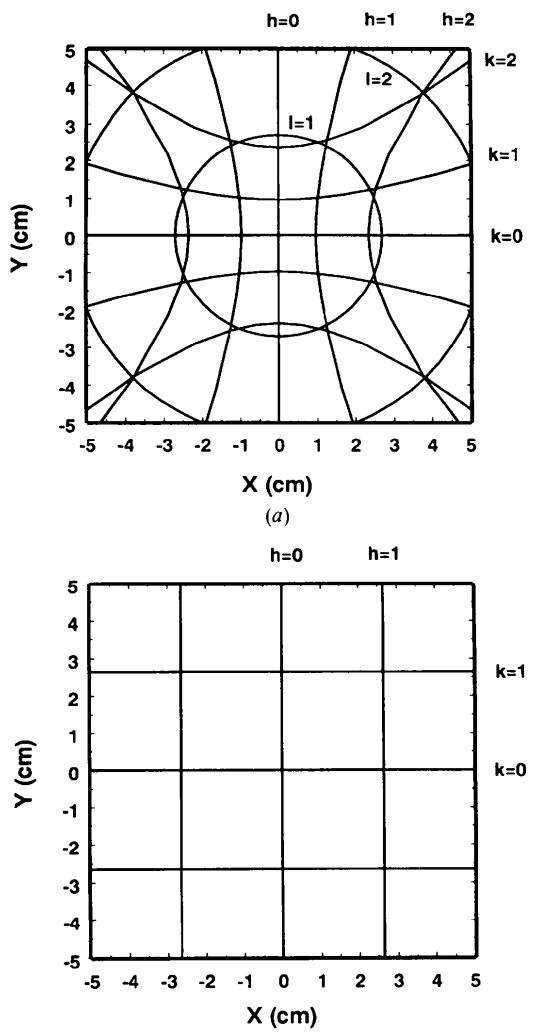

Fig. 2. Indexation diagrams for a tetragonal crystal with the c axis parallel to the direct beam at (*a*) $E_1 = 60$ keV and (*b*) $E_2 = 8.6$ keV. The parameters were $a = 5$, $b = 5$ and $c = 6$ Å; $d_1 = 63$ and $d_2 = 3$ cm.

in which D is the distance from the sample to the film, λ is the incident wavelength and h and k are the Miller indices. The intersection of the $00l$ reciprocal-lattice plans with the Ewald sphere will give rise to circles that in projection on the plane of the film will also be circles having a radius given by:

$$R(l) = D\tan[\arccos(1 - l\lambda/c)]. \qquad (2)$$

A Bragg reflection is observed on the film whenever the three lines intersect simultaneously. In the limit of small λ (that is to say at high energies), these expressions are reduced to

$$\begin{aligned} x(h,k) &= Dh\lambda/a \\ y(h,k) &= Dk\lambda/b \end{aligned} \qquad (3)$$

and only the $l=0$ scattering plane is observed.

In Fig. 2, we show a representation of such diagrams for two specific cases: (*a*) $\lambda = 1.54$ Å, $D = 3$ cm; (*b*) $\lambda = 0.21$ Å and $D = 63$ cm with the particular choice $a = b = 5$ and $c = 6$ Å. It is clear that the degree of complexity of the recorded pattern is quite different in the two cases. The complexity is directly related to the radius of the Ewald sphere, *i.e.* $1/\lambda$. At high energies (Fig. 2*b*), the radius becomes extremely large and one observes an undistorted image of the $l=0$ reciprocal-lattice plane. The indexation diagram then consists of straight lines. At smaller energies, (Fig. 2*a*), different $00l$ planes intersect the Ewald sphere, as shown by the presence of the circles in the figure. In this case, only the 121, 211 and 222 reflections with their equivalent symmetry-related reflections are observable. We note that, in contrast to what is observed for high incident energies, none of the $l=0$ reflections are observed. This demonstrates that by tuning the wavelength one can enlarge the Ewald sphere and bring any of the Bragg reflections of the fixed crystal in contact with the Ewald sphere.

As illustrated in the above discussion, the interpretation of the high-energy monoLaue pattern is straightforward since the indexation diagram consists only of straight lines. In addition, it is also extremely easy to record the different reciprocal-lattice planes belonging to the same zone axis since a simple rotation about the zone axis is all that is necessary to bring the required scattering plane into coincidence with the flat Ewald sphere. As an example, we have recorded the three $KMnF_3$ scattering planes, the (001), ($\bar{1}01$) and ($\bar{1}03$) planes, each belonging to the same 010 zone axis. The high-temperature phase of $KMnF_3$ is cubic with $a = 4.186$ Å and, with the beam parallel to the [001] direction, the three planes are brought into coincidence with the Ewald sphere by rotations of 0, 45 and 18.4° about the zone axis. Typical patterns for each of these planes are presented in Fig. 3. The patterns were recorded with the crystal held fixed and an exposure time of 150 s.

It is clear from Fig. 3(*a*) that we do indeed get a square reciprocal lattice in which all the Bragg reflections from the $l=0$ scattering plane are present as expected. The Bragg reflections are quite broad because the crystal was not oscillated. In addition, diffuse scattering at the position $\frac{1}{2}, \frac{3}{2}, 0$, which is an M point of the cubic

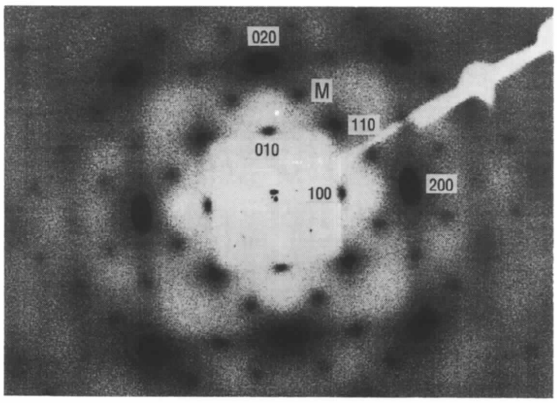

(*a*)

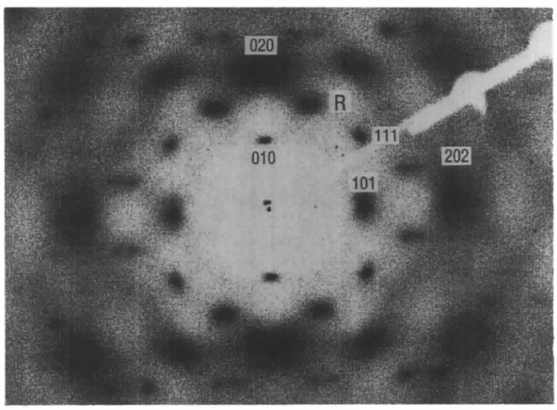

(*b*)

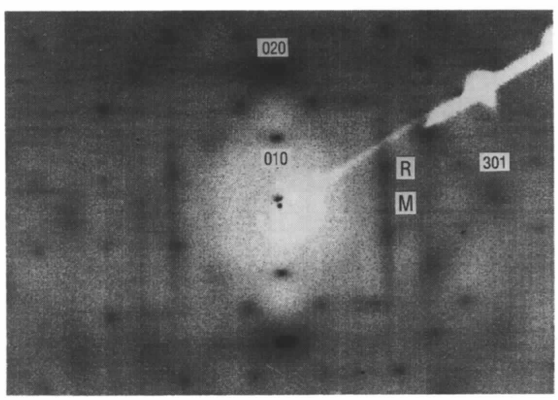

(*c*)

Fig. 3. High-energy X-ray monoLaue patterns of the (001), ($\bar{1}01$) and ($\bar{1}03$) scattering planes. (*a*) the [010] direction is vertical and the [100] direction is horizontal. (*b*) the [010] direction is vertical and the [101] direction is horizontal. (*c*) the [010] direction is vertical and the [301] direction is horizontal.

Brillouin zone, is clearly visible. The cubic Brillouin zone is presented in Fig. 4. The presence of this diffuse scattering is related to the existence in the perovskite compound of the flat RM branch of soft phonons, which has been extensively investigated in the past (Comès, Dénoyer, Deschamps & Lambert, 1971; Shapiro, Axe, Shirane & Riste, 1972; Almairac, Rousseau, Gesland, Nouet & Hennion, 1977; Cox & Cussen, 1989). A similar effect is observed in Fig. 3(*b*), where this time we pick up the *R* points of the Brillouin zone, for example $\frac{1}{2}, \frac{3}{2}, \frac{1}{2}$. Note the absence of diffuse scattering at the position $\frac{1}{2}, \frac{1}{2}, \frac{1}{2}$, where the structure factor is zero. The main advantage of utilizing high-energy X-rays for this kind of study is that one can really select any reciprocal plane of the zone axis. This allows us to bring the [301] direction into the scattering plane and we are able to record the entire *RM* line as shown in Fig. 3(*c*). Such a scattering plane was previously studied in some neutron scattering experiments (Almairac, Rousseau, Gesland, Nouet & Hennion, 1977) but, to our knowledge, this is the first time that this it has been examined in an X-ray scattering experiment. The reason for this is the fact that recent X-ray experiments in which diffuse scattering was measured were performed in reflection on the extended face of a single crystal with a two-circle goniometer (Andrews, 1986; Nicholls & Cowley, 1987; Gibaud, Ryan & Nelmes, 1987). Since perovskite crystals naturally cleave along the [100] directions, it is impossible to investigate this *RM* line in such a scattering geometry. At high energy and in transmission, the experimental conditions are similar to those encountered in neutron scattering experiments and it was possible with our set-up to study this line as a function of temperature.

It is well known that $KMnF_3$ undergoes three phase transitions at 186.5, 90 and 88.5 K (Gibaud, Shapiro, Nouet & You, 1991) and, as is the case for many perovskites of the type ABX_3, $KMnF_3$ undergoes these phase transitions by rotation of the MnF_6 octahedra. In this compound, the rotations are related to the softening of phonons, first at the *R* point, and then at the *M* point of the cubic Brillouin zone. A condensation at the *R* point is the signature that the octahedra have rotated in opposite directions in two consecutive planes, whereas one at the *M* point means that the octahedra have rotated in the same sense. X-ray diffuse scattering experiments first showed that a soft branch of phonons existed between the *R* and *M* points (Comès, Dénoyer, Deschamps & Lambert, 1971) and inelastic neutron scattering experiments confirmed that the entire *RM* branch is soft in the cubic phase and that the *R* point condenses first at 186.5 K. Clearly, then one would like to follow the behaviour of this entire line as a function of temperature through the different phase transitions.

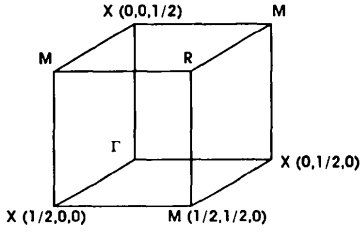

Fig. 4. The cubic Brillouin zone of $KMnF_3$.

In Fig. 5, we present the high-energy X-ray scattering patterns at 200, 186 and 75 K for the $(\bar{1}30)$ scattering plane. The crystal was oscillated with an amplitude of 4° during the exposure time of 150 s. In these figures, the presence of diffraction rings is clearly observed. These rings arise from the powder structure of the beryllium can used as a window in the cryostat. One set of rings is due to the front part of the can, while the second set comes from the back of the can with respect to the incident beam. Since these rings have an intensity that does not evolve with temperature, they are extremely useful as an on-line calibration of the intensity in a quantitative experiment. Indeed, one of the problems of the synchrotron experiments is the difficulty in obtaining absolute intensities. We also note a significant contamination of the diagram by the radiation of wavelength $\lambda/2$ which is clearly visible at the *M* point in Figs. 5(*a*) and (*b*). This contamination is related to the fact that we have used an Si 220 monochromator.

In Fig. 5, a significant evolution of the scattered intensity along the *RM* line is clearly observed as the temperature is progressively decreased. At 200 K (Fig. 5*a*), we observe some intensity along the entire length of the *RM* line. The intensity is enhanced at the *R* point as a result of the overlap with the perpendicular *RM* line. At 186 K, the *R* point has condensed into a tetragonal Bragg reflection, but at the same time some diffuse scattering is still clearly visible along the *RM* line (Fig. 5*b*). The diffuse intensity is quite visible down to 100 K and suddenly disappears when the second transition is passed (Fig. 5*c*) and the *M* point condenses. This aspect of phase transition has not been observed previously and neatly illustrates the utility of this simple technique. In particular, it demonstrates that a survey of reciprocal space can be extremely useful and complementary to more precise experiments where only a small part of reciprocal space is analyzed.

Finally, we note that image-plate patterns also contain quantitative information both in terms of location in reciprocal space and of measured intensities. This quantitative information is directly given by the reading device. In this study, the data after processing covered a dynamic range of only four orders of magnitude with a high level of background. As a result, extraction of reliable quantitative information on the diffuse scattering was not possible. This poor dynamical range was unfortunately limited by the device that reads the image plates, so that at the present time an improvement of the results can only be achieved by reduction of the

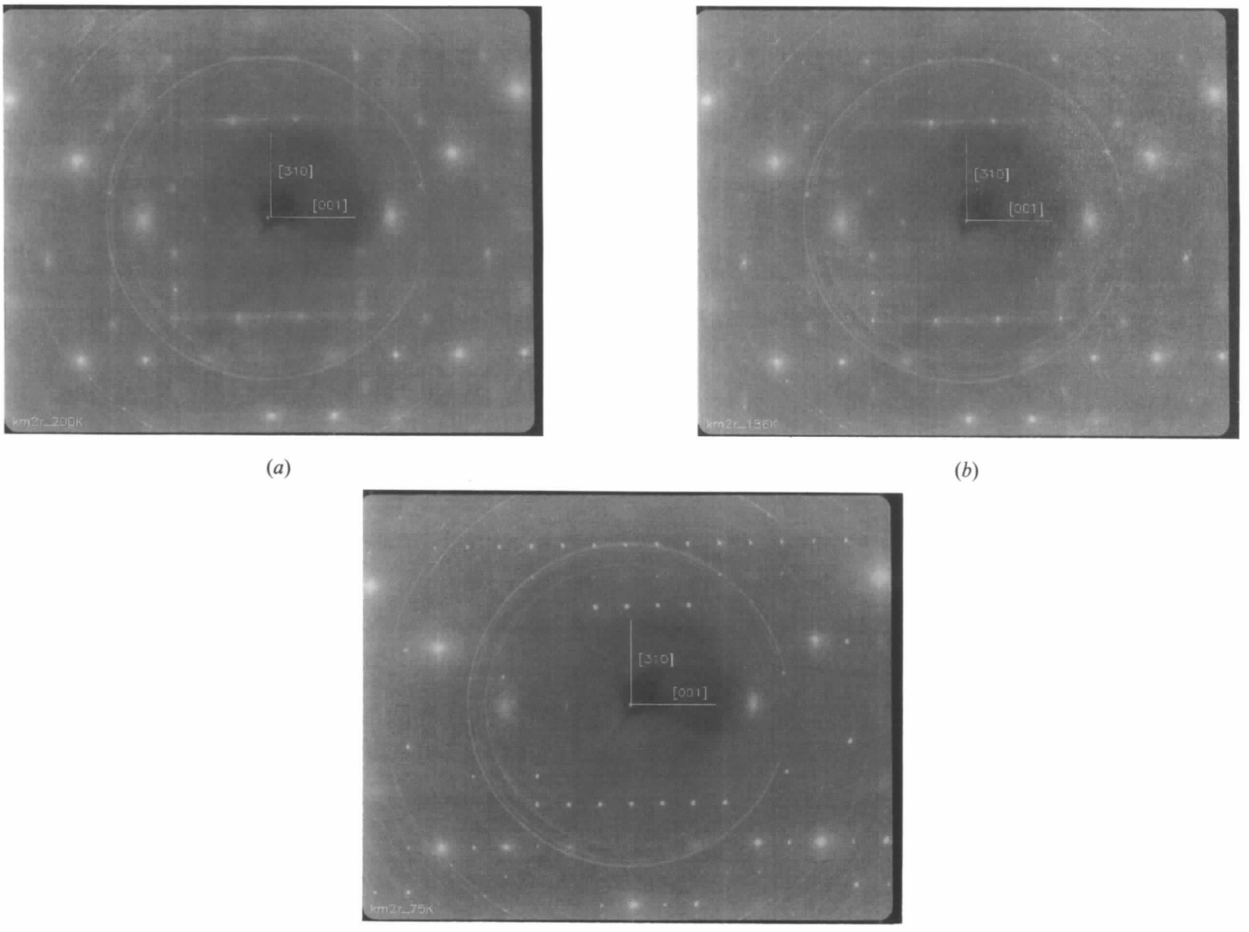

Fig. 5. High-energy X-ray monoLaue patterns of the ($\bar{1}30$) scattering plane at (*a*) $T = 200$ K, (*b*) $T = 186$ K and (*c*) $T = 75$ K showing the evolution of the intensity along the *RM* line.

background level. We plan to perform experiments in which more attention is paid to reducing the background level in the near future. Another limitation of the technique is related to the possibility of recording only the scattering planes which contain the origin of the reciprocal space. In the study of phase transitions, it is sometimes valuable to record parallel planes of the same family and the use of a precession camera is then necessary as recently demonstrated by Launois, Fettweis, Dénoyer & Lambert (1994).

This work was supported by the DOE under contract no. DE-ACO2-76CH00016.

References

Almairac, R., Rousseau, M., Gesland, J. Y., Nouet, J. & Hennion, B. (1977). *J. Phys.* **38**, 1429–1434.

Andrews, S. R. (1986). *J. Phys. C*, **19**, 3721–3743.

Comès, R., Lambert, M. & Guinier, A. (1970). *Acta Cryst.* A**26**, 244–249.

Comès, R., Dénoyer, F., Deschamps, L. & Lambert, M. (1970). *Phys. Lett.* **34**A, 65–68.

Cox, U. & Cussen, L. D. (1989). *J. Phys. Condensed Matter*, **1**, 3579–3589.

Dénoyer, F., Comès, R. & Lambert, M. (1970). *Solid State Commun.* **8**, 1979–1981.

Dénoyer, F., Comès, R., Lambert, M. & Guinier, A. (1974). *Acta Cryst.* A**30**, 423–430.

Gibaud, A. (1987). Doctoral thesis, University of Maine, France.

Gibaud, A., Bulou, A., Launay, C. & Nouet, J. (1987). *J. Phys. (Paris)*, **48**, 625–633.

Gibaud, A., Ryan, T. W. & Nelmes, R. J. (1987). *J. Phys C*, **20**, 3833–3848.

Gibaud, A., Shapiro, S. M., Nouet, J. & You, H. (1991). *Phys. Rev. B*, **44**, 2437–2443.

Launois, P., Fettweis, M., Dénoyer, F. & Lambert, M. (1994). *Europhys. Lett.* **26**, 595–600.

Nicholls, U. J. & Cowley, R. A. (1987). *J. Phys. C*, **20**, 3417–3427.

Shapiro, S. M., Axe, J. D., Shirane, G. & Riste, T. (1972). *Phys. Rev. B*, **6**, 4332–4341.